International Journal of Bifurcation and Chaos

Modeling, Dynamics, Bifurcation Behavior and Stability Analysis of a DC-DC Boost Converter in Photovoltaic Systems

Meriem Zhioua
École Nationale d'Ingénieurs de Tunis (ENIT),Université de Tunis El Manar , Tunis, Tunisia
maryoumazhioua@gmail.com

Abdelali El Aroudi
Departament d'Enginyeria Electronica, Electrica i Automatica, Universitat Rovira i Virgili, Tarragona, Spain
abdelali.elaroudi@urv.cat

Safya Belghith
École Nationale d'Ingénieurs de Tunis (ENIT), Université de Tunis El Manar , Tunis, Tunisia
safyabelghith@yahoo.fr

Joseph M. Bosque-Moncusí, Roberto Giral
Departament d'Enginyeria Electronica, Electrica i Automatica, Universitat Rovira i Virgili, Tarragona, Spain

K. Al Hosani
Department of Electrical Engineering, The Petroleum Institute, Abu Dhabi, UAE

M. Al-Numay
Department of Electrical Engineering, King Saud University, Riyadh, KSA

Received (to be inserted by publisher)

A study is presented of a DC-DC boost converter fed by a PV generator and supplying a constant voltage load. The input port of the converter is controlled using fixed frequency pulse width modulation (PWM) based on the loss free resistor (LFR) concept whose parameter is selected with the aim to force the generator to work at its maximum power point. Under this control strategy, it is shown that the system can exhibit complex nonlinear behaviors for certain ranges of the parameter values. First, using the nonlinear models of the converter and the PV source, the dynamics of the system are explored in terms of some of its parameters such as the proportional gain of the controller and the output DC bus voltage. To present a comprehensive approach of the overall system behavior under parameter changes, a series of bifurcation diagrams are computed from the circuit-level switched model and a simplified model obtained under some realistic approximations both implemented in PSIM© software getting a remarkable agreement. These diagrams show that the fist instability that takes place in the system period-1 orbit when a primary parameter is varied is a smooth period doubling bifurcation and that the nonlinearity of the PV generator is irrelevant for predicting this phenomenon. Different bifurcation scenarios can take place for the resulting period-2 subharmonic regime depending on a secondary bifurcation parameter. The boundary between the desired period-1 orbit and subharmonic oscillation resulting from period doubling in the parameter space is obtained by calculating the eigenvalues of the monodromy matrix of the simplified model. The results from this model have been validated with time-domain numerical simulation using the circuit-level switched model and also experimentally from a laboratory prototype. This study can help in

selecting the parameter values of the circuit in order to delimit the region of period-1 operation of the converter which is of practical interest in PV systems.

Keywords: PV-fed boost, loss-free resistor (LFR), modelling, period doubling, chaos, stability analysis.

1. Introduction

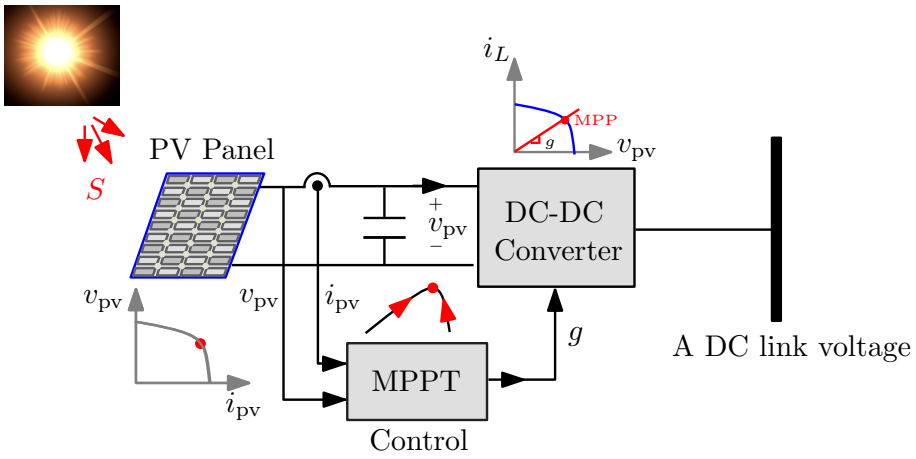

Fig. 1. PV-fed boost converter behaving as LFR loaded by a constant DC voltage representing a DC bus such as battery or a DC link.

Photovoltaic power generation (PV) has gained considerable interest over the past two decades due to its clean-energy property and its inexhaustibility. However, the power energy produced from PV panels is naturally variable and largely dependent on the climatic changes. Connecting a PV module to charge a constant voltage battery or using it to feed resistive loads or grid connected inverters, requires always the presence of a power converter as an interface to adapt the energy flow between the source and the load sides. The main requirement of power electronic interfaces in PV systems is to convert the generated DC voltage into a suitable AC for consumer use and utility connection in AC distribution systems or connected directly to the main DC bus in DC distribution systems, Fig.1. In both cases, the role of the power converter is mainly to extract the maximum power from the PV source [Xiao *et al.* , 2007]. PV grid-connected power systems in residential applications are already becoming popular in many countries [epia , 2014]. Unfortunately, the output voltage of the PV arrays is relatively low and a step-up voltage converter must be used in this kind of applications to rise the DC voltage magnitude to a sufficient level before connected to the AC or DC distribution system. Although, many voltage step-up switching power conversion circuits can be a candidate for power processing, one of the most used topologies in these applications is the elementary boost converter [Xiao *et al.* , 2007; Leyva *et al.* , 2007; Yang *et al.* , 2012; Chiu *et al.* , 2011; Garcer *et al.* , 2012]. In PV applications, the input port is regulated via a suitable feedback to extract the maximum available power from the PV generator. In practice, the desired behavior in these systems is a periodic orbit with the same period of the sampling PWM period T, which is in turn equal to that of an external clock signal. Unfortunately, the switching nonlinearity of power converters can put their stability at risk and make them prone to exhibit various nonlinear instability phenomena that can have harmful effects on the converter and the devices that it interconnects and may cause system failure, mal malfunctioning or even damages caused by the increase of the stress on the switching components which would rise the working temperature and this in turn would shorten the lifetime of the system. The system can even enter through different bifurcation scenarios into chaotic regimes. Therefore, their study and prediction are important from both a theoretical and a practical point of view. The most commonly

encountered instabilities in power converters are Hopf (slow-scale) bifurcation, and the period-doubling (fast-scale) bifurcation. Both kinds of instabilities result in the loss of stability of the desired period-1 orbit and the emerging of either a slow scale oscillation in the form of quasiperiodic behavior in the first case or subharmonic oscillation in the second case. These instabilities or bifurcations have interested researchers since the pioneer works of Deane and Hamill and coworkers [Deane , 1992; Deane & Hamill , 1990; Deane, J. & Hamill , 1990; Deane & Hamill , 1991] and since then a large amount of work in this area was reported during the last decades [Dénes & Nagy , 2003; Fossas & Olivar , 1996; Banerjee & Verghese , 2001; El Aroudi *et al.* , 2005; Banerjee & Chakrabarty , 1998; El Aroudi & Leyva , 2001; Zhusubaliyev *et al.* , 2003; Chan & Tse , 1997; Cafagna & Grassi , 2006; Pikulin , 2014; Zamani *et al.* , 2015; Xiong *et al.* , 2013]. A review of the different instabilities phenomena that can be undergone by the desired steady-state solution and the different techniques that can be used to detect them can be found in [El Aroudi *et al.* , 2005, 2015]. The previous studies, which are mostly based on accurate approaches such as discrete-time mappings [El Aroudi *et al.* , 2005] or the Floquet theory combined with *Filippov's method* [Giaouris *et al.* , 2008, 2009; Giaouris *et al.*, 2013], have allowed a deep understanding of the mechanisms of losing stability in these systems. However, most of the previous works existing in the literature consider voltage-fed converters with resistive loads. In PV applications, the converter is fed by a nonlinear source and it is usually loaded by a constant voltage load [Xiao *et al.* , 2007; Leyva *et al.* , 2007]. In this particular situation, unlike classical converters, the output voltage of the PV-fed boost converter is imposed either by a dc storage device (e.g. battery), or by a dc-ac grid-connected inverter. In both cases, the output voltage of the boost converter is practically constant. An important direction in the study of the nonlinear behavior of power electronics circuits and systems could be on focusing on the mechanisms of losing stability of the system period-1 orbit to gain insights of commonly used practical power electronics systems with real power sources and loads [Tse & Li , 2011]. In [Al-Hindawi *et al.* , 2014] the authors analyze the dynamics of boost converter supplied with a real nonlinear PV source. However, in that work the input capacitance was not included in the system dynamics. The use of such a capacitance is mandatory for smoothing the input voltage to be used by the maximum power point tracking (MPPT) control algorithm and also to avoid injecting high frequency current ripple to the PV panels and its connecting wires (high radiated EMI). In [Abusorrah *et al.* , 2013], the authors explore the dynamics and stability of a PV-fed boost converter with a resistive load. It has been shown both by theoretical results and experimentally that the nonlinear PV generator combined with the battery's output voltage variation can increase or decrease the converter's stability range. A conflict between stability and efficiency was also reported.

Accurate modeling, simulation and stability analysis are indispensable for the design of these converters. A trade off always exists between simplicity and accuracy of the models. A model must be simple to allow design-oriented analysis of the dynamical behavior and at the same time not so simple that details of the system behavior are lost. The design of switching converters for PV systems with a nonlinear PV source would require to know suitable ways of approximating the system to get some design guidelines to predict subharmonic oscillation instabilities and to delimit the stability region in the parameter space and finally some design guidelines. This paper takes the first step in achieving these objectives. Some initial study by the authors was presented in [zhioua *et al.* , 2015]. In the present paper we thoroughly expand the previous analysis and fully study the originally reported phenomena. In particular, we consider a PV-fed boost converter loaded by a constant voltage for PV applications. The relevant parasitic parameters existing in practice are included in the circuit. The control of the converter has been carried out using a pulse width modulator (PWM) strategy in such a way that the input port of the converter behaves as a loss free resistor (LFR) in average [Shmilovitz , 2005; Cid-Pastor *et al.* , 2010] hence improving the stability at the slow scale [Haroun *et al.* , 2014, 2015]. Bifurcation diagrams have been plotted using the switched circuit-level model implemented PSIM© and from a simplified discrete-time model getting a remarkable agreement. The simplified discrete-time model is then used to analyze accurately the occurrence of the first instability in the PV system. Based on the simplified model, stability analysis is then addressed by using Floquet theory and the monodromy matrix [Giaouris *et al.* , 2008, 2009; Giaouris *et al.*, 2013]. The characteristic multipliers are calculated and the first onset of period-doubling bifurcation is predicted, as well as the stable region of the system operation is defined. Experimental tests performed for the considered system are in good agreement with PSIM© simulations.

The rest of this paper is organized as follows. Section 2 describes the proposed PV-fed boost converter. Section 3 presents the dynamical model of the system. Section 3 explores the dynamics and stability of the PV system under PWM using the nonlinear model of the PV generator and from a simplified model consisting of substituting this generator by a linear current source. Both switched circuit-level models are implemented in PSIM©. Bifurcation diagrams have been computed from both models and a good agreement has been obtained. In section 4, the mathematical model of the system in the form of a state-space description is addressed. Section 5 deals with the derivation of a simplified discrete-time model of the system which has been used in Section 6 to obtain the the monodromy matrix, its eigenvalues and the domain of stability in the parameter-space. Experimental validation is provided in section 7. Finally, the conclusions of this study are presented in the last section.

2. PV-fed boost converter based LFR under PWM strategy

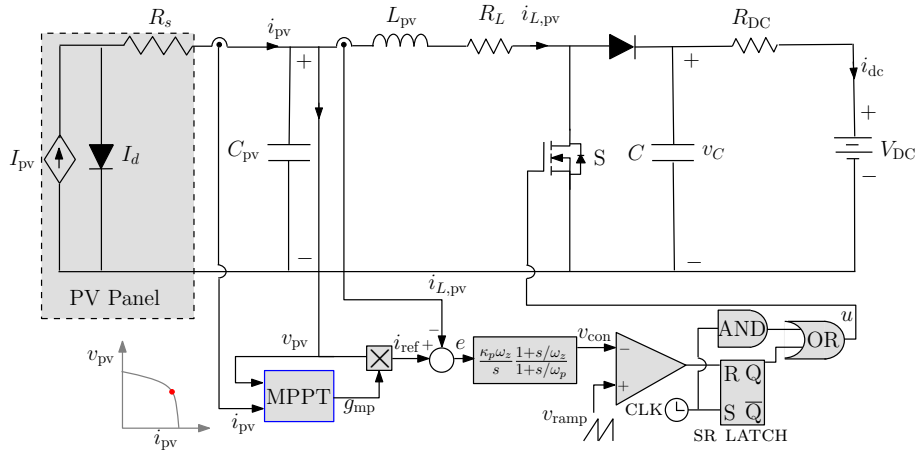

Fig. 2. Schematic diagram of a PV-fed boost converter behaving as an LFR under PWM strategy.

The proposed PV power conversion system is presented in Fig.2. The power processing unit is a DC-DC boost converter with an additional input capacitor, fed by a PV panel and loaded by a constant voltage. The DC-DC converter in PV applications is mainly responsible for tracking the maximum power point (MPPT) by controlling its input variables. In this study, an output capacitance filter is employed to reduce the switching ripple and to provide a smooth current $i_{\rm DC}$ to the output DC bus. The power converter stage is controlled to behave as an LFR under fixed frequency pulse width modulating (PWM) strategy by generating a current reference $i_{\rm ref}$ proportional to the input voltage $v_{\rm pv}$. The proportionality factor of the LFR is supposed to be provided by the MPPT controller [Haroun *et al.* , 2014, 2015]. The goal of the MPPT is to ensure that the PV module always operates at its MPP regardless of the temperature, insolation and load variation. The MPPT controller aiming to provide the parameter g is an entirely separate issue and is not taken into account in this study. However, the value of g is always selected to evolve around the optimum value $g_{\rm mpp} = i_{\rm mpp}/v_{\rm mpp}$, where $i_{\rm mpp}$ and $v_{\rm mpp}$ are, respectively, the PV current and PV voltage at the maximum power point. The ON/OFF binary driving signal u for the switch S is generated by a comparator, set-reset (SR) latch and logic AND and OR gates as shown in Fig.2. The duty cycle is generated according to the error e between the input current $i_{L,\rm pv}$ and its desired reference $i_{\rm ref} := g_{\rm mpp} v_{\rm pv}$. The error signal is processed by means of a type-II compensator having a pole at the origin to get a zero static error, a low frequency zero with corner frequency ω_z to increase the phase margin and a pole with corner frequency ω_p to reduce noise due to the switching action. The transfer function of the previous controller can be expressed in the $s-$domain as follows:

$$H_c(s) = \frac{\kappa_p \omega_z}{s} \frac{1 + s/\omega_z}{1 + s/\omega_p} \tag{1}$$

where κ_p is the proportional gain of the controller, ω_z its zero and ω_p its pole. The control logic works as follows. The comparator compares cyclically the control signal v_{con} with the ramp signal v_{ramp} whose lower value is V_l and upper value is V_u. If at the start of a switching cycle $V_l < v_{\text{con}}(nT) < V_u$, the clock signal sets the SR latch at the starting of the clock signal and the comparator resets the SR latch when the signals v_{con} and v_{ramp} intersect forcing the signal u to be high and the switch to turn ON. If within the same switching cycle the signals v_{con} and v_{ramp} do not intersect, the switch is maintained ON during all this cycle. If at the start of a switching cycle $v_{\text{con}}(nT) < V_l$, the SR latch is high for a short period equal to the width of the clock signal and it is reset during the whole remaining period during the same switching cycle. Fig. 3 shows the different cases described previously.

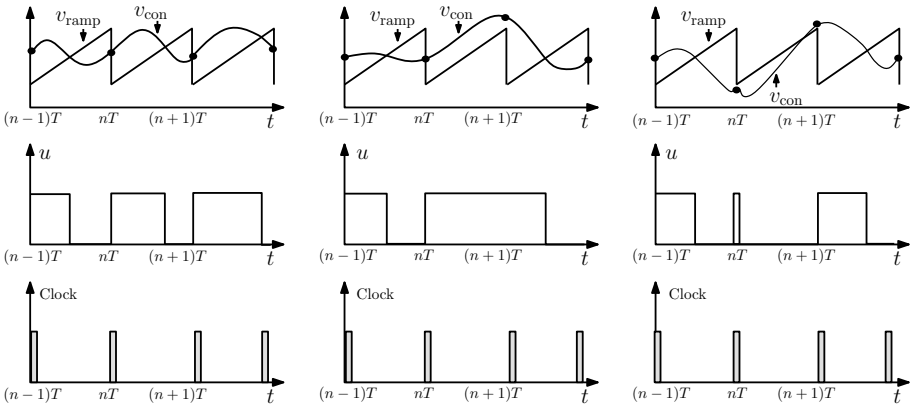

Fig. 3. Different switching patterns according to the waveforms of the control signal v_{con} at time instants nT.

3. Behavior of the PV system: Simulation results from PSIM© software

In this section, the dynamical behavior of the PV system is explored in order to gain insight on suitable ways of obtaining appropriate models that can be used for stability analysis and ultimately for design purposes. First, the system has been carefully studied through simulations using the nonlinear model of the PV generator. A series of bifurcation diagrams have been obtained using the exact switched circuit-level model of PSIM© by varying the proportional gain κ_p and considering different values of the output DC bus voltage V_{DC}. The fixed parameter values used for this study are reported in Table 1. For simplicity, the dynamics of the MPPT algorithm is neglected because it is usually much slower than the converter dynamics and its output, the proportionality factor g, is set equal to the optimum value g_{mpp} that should be achieved this controller. However, numerical simulations will be provided later by including the MPPT controller. The used solar module has an open-circuit voltage v_{oc} equal to 22.1 V and a short circuit current I_{sc} around 5 A based on the data of BP585 [BP585 , 2015], its internal parameters being shown in Table 2. It is also worth mentioning that the input voltage depends on weather conditions and and it is inferior than the open circuit voltage with a nominal value of approximately 18 V at the MPP which barely varies with irradiation.

Herein, we investigate the change in dynamics of the system as the proportional gain κ_p and the output DC bus voltage vary for different values of the DC bus voltage V_{DC}. A convenient way of having a panoramic view of the stability status under the varying parameters without any mathematical analysis and using the nonlinear model of the system is through bifurcation diagrams. In obtaining such diagrams a suitable variable is sampled at every clock instant and the corresponding data is represented when a parameter varies. If the system exhibits a periodic period-1 in steady-state regime, all the sampled points will have the same value and they will represent a single point single point. When period-2 subharmonic regime takes place in steady-state, one gets two points instead of one, and so on... In this study, the bifurcation diagrams are obtained by computing the duty cycle d_n at every switching cycle nT, $n = 0, 1 \ldots 2000$. Time transient is eliminated and the last 150 samples are considered as steady-state. The duty cycle is plotted when the bifurcation parameter κ_p is varied. The results are shown in Fig. 5. It can be observed that we

C_{pv}	43 μF
L_{pv}	200 μH
R_L	100 mΩ
C	204 μF
V_{DC}	variable
R_{DC}	200 mΩ
g_{mpp}	275 mS
T	20 μs
$\tau = 1/\omega_z$	1 ms
κ_p	variable
w_p	175 krad/s
V_u	1 V
V_l	0 V

Parameter	Value
Maximum Power (P_{max})	85 W
Voltage at P_{max} (V_{mp})	18 V
Current at P_{max} (i_{mpp})	4.72 A
Short circuit current I_{sc}	5 A
Open circuit voltage v_{oc}	22.1 V
Temperature T_{ref}	25 ^{o}C

get qualitatively similar bifurcation structure mechanism, independently of wether the exact model or the simplified model is used. In both cases it can be observed that the converter exhibits first a period doubling bifurcation at certain value of κ_p. It is clear that for values of the proportional gain κ_p less than a critical value depending on the DC bus output voltage the converter operates in the stable period-1 regime. At this critical value the system undergoes a period doubling (PD) bifurcation and a period-2 orbit emerges. The resulting period-2 orbit undergoes a non-smooth border or collision (BC) bifurcation, [Banerjee *et al.* , 1997, 2000; Robert & Robert , 2002; Wolf *et al.*, 1994], as depicted in Fig. 4. Namely, it can be observed that at another critical value of κ_p, the period-2 orbit collides with the one of the borderlines $d_n = \delta$ or $d_n = 1$. For relatively low values of the output DC bus voltage, the lower borderline $d_n = \delta$ is usually reached before the upper borderline $d_n = 1$ and the system undergoes a persistence bifurcation. In this case, the period-2 orbit does not change its periodicity but one of its branches is saturated with a duty cycle $d_n = \delta \; \forall n$. If the output DC bus voltage increases, the upper borderline $d_n = 1$ could be reached before the lower one and different scenarios can take place. For instance, for $V_{\text{DC}} = 48$ V, the period-2 undergoes a BC giving rise to a period-4 orbit which in turns undergoes a series period doubling culminating in a chaotic attractor close to $\kappa_p = 2.2$. One can observe that at $\kappa_p \approx 1.4$, one of the branches of the period-2 orbit hits the borderline V_u of the dynamical system giving rise to a border collision bifurcation. At this point, one of the branches of the period-2 orbit is saturated since one of its corresponding duty cycles is equal to 1. As the bifurcation parameter is increased further, period-8 orbit emerges which undergo a border collision resulting in a chaotic attractor. The period-orbit can hit the upper borderline and the system can enter into the chaotic regime directly. This is the case of $V_{\text{DC}} = 180$ V.

In order to check the results obtained from bifurcation diagrams, time domain simulations have been carried out by the switched circuit-level model implemented in PSIM© software.

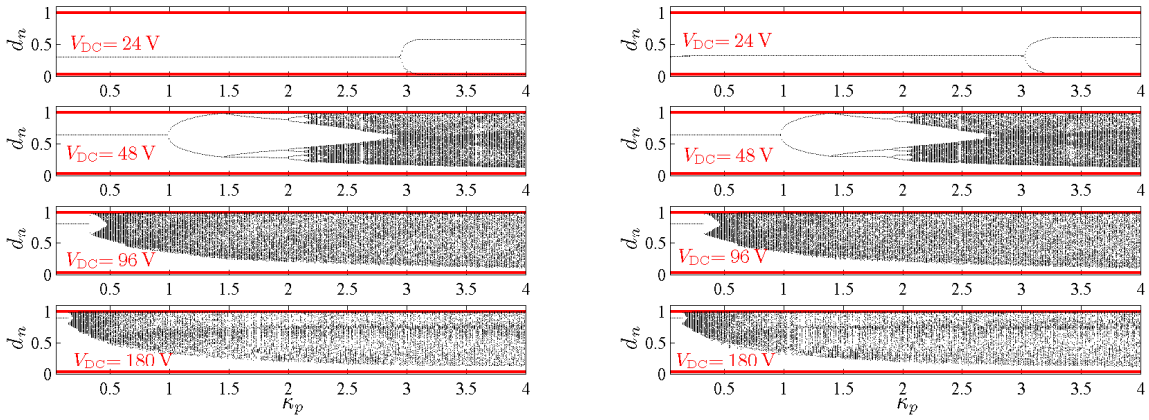

(a) (b)

Fig. 4. Bifurcation diagram of the PV-fed boost converter showing the duty cycle by taking the proportional gain κ_p as a bifurcation parameter for different values of the bus voltage V_{DC}. (a) Using the nonlinear PV model. (b) Using the constant current source model.

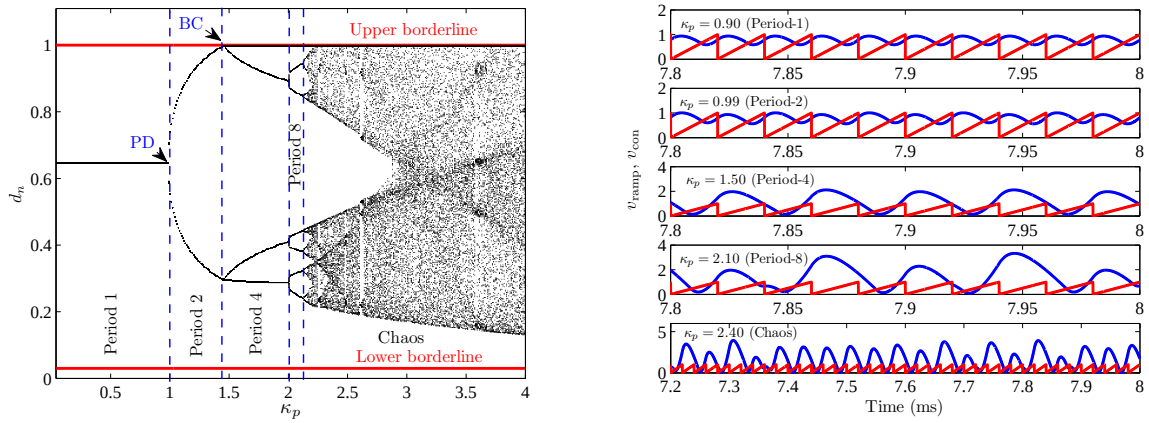

(a) (b)

Fig. 5. (a) Bifurcation diagram of the PV-fed boost converter showing the duty cycle d_n at time instants nT by taking the proportional gain κ_p as a bifurcation parameter. $V_{\mathrm{DC}} = 48$ V. (b) Time domain waveforms of the control voltage v_{con} and the ramp signal v_{ramp} for different values of κ_p

4. Continuous-time modeling of the PV system

By applying Kirchhoff's voltage and current laws to the circuit presented in Fig. 2, the following set of differential equations describing the dynamical behavior of the PV-fed boost converter are obtained:

$$\frac{\mathrm{d}v_{\mathrm{pv}}}{\mathrm{d}t} = \frac{i_{\mathrm{pv}}}{C_{\mathrm{pv}}} - \frac{i_{L,\mathrm{pv}}}{C_{\mathrm{pv}}} \tag{2a}$$

$$\frac{\mathrm{d}i_{L,\mathrm{pv}}}{\mathrm{d}t} = \frac{v_{\mathrm{pv}}}{L_{\mathrm{pv}}} - \frac{R_L}{L_{\mathrm{pv}}} i_{L,\mathrm{pv}} - \frac{v_C}{L_{\mathrm{pv}}}(1-u) \tag{2b}$$

$$\frac{\mathrm{d}v_C}{\mathrm{d}t} = \frac{V_{\mathrm{DC}} - v_C}{R_{\mathrm{DC}} C} + \frac{i_{L,\mathrm{pv}}}{C}(1-u) \tag{2c}$$

where u is the driving signal that takes values in the $\{0, 1\}$ set, L_{pv} is the inductance of the inductor, R_L is the DC resistance of the inductor, C_{pv} is the capacitance of the input capacitor, C is the output capacitance filter, R_{DC} is the bus resistance, $i_{L,\text{pv}}$ is the inductor current, v_{pv} is the input capacitor voltage, v_C is the output capacitor voltage, i_{pv} is the current delivered by the PV panel, and V_{DC} is the bus voltage. The state equations corresponding to the input type-II controller can be expressed as follows:

$$\frac{\mathrm{d}v_e}{\mathrm{d}t} = gv_{\text{pv}} - i_{L,\text{pv}}, \tag{3a}$$

$$\frac{\mathrm{d}v_{\text{con}}}{\mathrm{d}t} = -\omega_p v_{\text{con}} + \omega_p \kappa_p e + \kappa_p \omega_p \omega_z v_e. \tag{3b}$$

Under continuous conduction mode (CCM), the system switches sequentially between the two following configurations during one complete switching cycle:

$$\dot{\mathbf{x}} = \begin{cases} \mathbf{A}_1\mathbf{x} + \mathbf{B} & \text{for} \quad u = 1 \\ \mathbf{A}_0\mathbf{x} + \mathbf{B} & \text{for} \quad u = 0 \end{cases} \tag{4}$$

where $\mathbf{x} = (v_{\text{pv}},\ i_{L,\text{pv}},\ v_C,\ v_e,\ v_{\text{con}})^\intercal$ presents the vector of the state variables. The matrices $\mathbf{A}_1$, $\mathbf{A}_0$ and $\mathbf{B}$ and the feedback coefficients vector $\mathbf{K}$ are as follow:

$$\mathbf{A}_1 = \begin{pmatrix} 0 & \frac{-1}{C_{\text{pv}}} & 0 & 0 & 0 \\ \frac{1}{L_{\text{pv}}} & \frac{-R_L}{L_{\text{pv}}} & 0 & 0 & 0 \\ 0 & 0 & \frac{-1}{CR_{\text{DC}}} & 0 & 0 \\ g & -1 & 0 & 0 & 0 \\ \omega_p\kappa_p g & -\omega_p\kappa_p & 0 & \kappa_p\omega_p\omega_z & -\omega_p \end{pmatrix}, \tag{5a}$$

$$\mathbf{A}_0 = \begin{pmatrix} 0 & \frac{-1}{C_{\text{pv}}} & 0 & 0 & 0 \\ \frac{1}{L_{\text{pv}}} & \frac{-R_L}{L_{\text{pv}}} & -\frac{1}{L_{\text{pv}}} & 0 & 0 \\ 0 & \frac{1}{C} & \frac{-1}{CR_{\text{DC}}} & 0 & 0 \\ g & -1 & 0 & 0 & 0 \\ \omega_p\kappa_p g & -\omega_p\kappa_p & 0 & \kappa_p\omega_p\omega_z & -\omega_p \end{pmatrix}, \tag{5b}$$

$$\mathbf{B} = \begin{pmatrix} \frac{i_{\text{pv}}}{C_{\text{pv}}} \\ 0 \\ \frac{V_{\text{DC}}}{CR_{\text{DC}}} \\ 0 \\ 0 \end{pmatrix}, \qquad \mathbf{K} = \begin{pmatrix} 0 \\ 0 \\ 0 \\ 0 \\ 1 \end{pmatrix}^\intercal. \tag{5c}$$

.

5. Simplified Discrete-time modeling of the PV system

5.1. *General assumptions*

Three types of nonlinearities are present in the previous model. The first one is the switching nonlinearity of the converter. The second one is the nonlinear current-voltage characteristic of the PV generator. Its expression can be described as in [Villalva *et al.* , 2009; Haroun *et al.* , 2015]. The third one is the nonlinear dynamics of any MPPT controller. The discrete-time model can be obtained by integrating the previous continuous-time model and cascading the solutions at the switching instants. For the considered application, two of the previous nonlinearities are handicaps preventing from obtaining a closed form expression for the discrete-time model. The first one is the nonlinear model of the PV generator and the

implicit relationship between the PV voltage $v_{\rm pv}$ and its current $i_{\rm pv}$. The second one is the dynamics of the MPPT algorithm which usually based on heuristic rules rather than a mathematical model. To overcome these handicaps we will use some realistic assumptions. First, it is well known that the dynamics of the MPPT algorithm is much slower than that of the switching converter. The amplitude of oscillation of the optimal conductance $g_{\rm mpp}$ provided by this algorithm is also very small for any practical, efficient and well tuned MPPT controller. Hence the effect of the MPPT algorithm on the overall system dynamics is just to make the system to reach the MPP. Therefore, we assume that the MPPT controller provides a constant conductance value g which will be shown as a good approximation for the purpose of predicting subharmonic oscillation in steady-state regime. Hence, once the system is working at this point, the model of the PV generator can be substituted by a current source $i_{\rm mpp}$. This is a widely used approximation for designing DC-DC converters for PV applications [Leppäaho *et al.*, 2010; Leppäaho & Suntio, 2011]. Therefore, the vector fields between the switching events near the MPP can be considered linear close to this point, where the current of the PV panel and its voltage can be substituted by their optimal values. Therefore, we can use the exact analytical solution to express the value of the state vector at the end of a switching cycle in terms of its value at the beginning of that cycle. The local Poincaré map of the system within switching sub-intervals can be obtained by using solving (4) during the corresponding interval the resulting equations after substituting $i_{\rm pv}$ by $i_{\rm mpp}$.

5.2. *Derivation of the model*

Let us define $\mathbf{x}_n = \mathbf{x}(nT)$. The main objective is to obtain a Poincaré map $\mathbf{P}$ relating $\mathbf{x}_{n+1} = \mathbf{x}((n+1)T)$ to $\mathbf{x}_n = \mathbf{x}(nT)$. Let $\mathbf{x}_d = \mathbf{x}((n+d_n)T)$, $\mathbf{x}_{n+1} = \mathbf{x}((n+1)T)$ where d_n is the duty cycle during the cycle $(nT, (n+1))T$. Therefore one can write:

$$\mathbf{x}_d := \mathbf{P}_1(\mathbf{x}_n, d_n) = \mathbf{\Phi}_1(d_nT)\mathbf{x}_n + \mathbf{\Psi}_1(d_nT) \tag{6a}$$

$$\mathbf{x}_{n+1} := \mathbf{P}_0(\mathbf{x}_d, d_n) = \mathbf{\Phi}_0((1-d_n)T)\mathbf{x}_d + \mathbf{\Psi}_0((1-d_n)T) \tag{6b}$$

where $\mathbf{\Phi}_u(t)$ and $\mathbf{\Psi}_u(t)$ are defined by:

$$\mathbf{\Phi}_u(t) = e^{\mathbf{A}_u t} \quad \text{and} \quad \mathbf{\Psi}_u(t) = \int_0^t e^{\mathbf{A}_u \tau}\mathbf{B}\mathrm{d}\tau \tag{7}$$

The mapping describing the system behavior between the time instants nT and $(n+1)T$ can be obtained by composing the two previously presented local mappings [ElAroudi *et al.*, 2007], i.e., the Poincaré map $\mathbf{P} = \mathbf{P}_0 \circ \mathbf{P}_1$ of the switched PWM system described by the vector fields given in (4) can be written in the following form:

$$\mathbf{x}_{n+1} = \mathbf{P}(\mathbf{x}_n, d_n) \tag{8}$$

where $\mathbf{\Phi}(d_n)\mathbf{x}_n + \mathbf{\Psi}(d_n)$ and $\mathbf{\Phi}(d_n)$ and $\mathbf{\Psi}(d_n)$ are given by:

$$\mathbf{\Phi}(d_n) := \mathbf{\Phi}_0((1-d_n)T)\mathbf{\Phi}_1(d_nT) \tag{9a}$$

$$\mathbf{\Psi}(d_n) := \mathbf{\Phi}_0((1-d_n)T)\mathbf{\Psi}_1(d_nT) + \mathbf{\Psi}_0(d_nT) \tag{9b}$$

According to the control logic described previously in Section 2, different values of the duty cycle are possible and hence different expression for the discrete-time model arise. Namely, the different cases are:

- Case 1: If at the start of a switching cycle $\mathbf{K}\mathbf{x}_n < V_l$ the SR latch is high for a short period equal to the width of the clock signal and it is reset during the whole remaining time interval during the same switching cycle and the map will be described by:

$$\mathbf{x}_{n+1} = \mathbf{P}(\mathbf{x}_n, \delta) \tag{10}$$

where $\delta << 1$ is a small parameter representing the duty cycle of the clock forcing signal. This imposes a positive lower bound for the possible values of the duty cycle and defines a borderline in the state-space.

- Case 2: If at the start of a switching cycle $\mathbf{K}\mathbf{x}_n > V_l$ and $\mathbf{K}(\mathbf{\Phi_1}(T)\mathbf{x}_n + \mathbf{\Psi_1}(\mathbf{T})) < V_u$, the clock signal sets the SR latch at the starting of the clock signal and the comparator resets the SR latch when the signals v_{con} and v_{ramp} intersect. Hence the expression of the map will be as follows:

$$\mathbf{x}_{n+1} = \mathbf{P}(\mathbf{x}_n, d_n) \tag{11}$$

where $d_n = t_n/T$ and t_n is the conduction time during this cycle, which can be obtained by solving the following equation:

$$\mathbf{K}(\mathbf{\Phi_1}(t)\mathbf{x}_n + \mathbf{\Psi_1}(t)) - (V_l + (V_u - V_l)\frac{t}{T}) = 0 \tag{12}$$

- Case 3: If at the start of a switching cycle $\mathbf{K}\mathbf{x}_n > V_l$ and $\mathbf{K}(\mathbf{\Phi_1}(T)\mathbf{x}_n + \mathbf{\Psi_1}) > V_u$, the signals v_{con} and v_{ramp} do not intersect. In this case, the switch is maintained ON during all this cycle imposing a saturation of the duty cycle at its upper limit $d_n = 1$ defining another borderline in the state-space. The expression of the map in this case will be as follows:

$$\mathbf{x}_{n+1} = \mathbf{P}(\mathbf{x}_n, 1) \tag{13}$$

Hence the general expression of the map can be written in the following form:

$$\mathbf{x}_{n+1} = \begin{cases} \mathbf{P}(\mathbf{x}_n, \delta) = \mathbf{\Phi}_0(\overline{\delta}T)\mathbf{\Phi}_1(\delta T)\mathbf{x}_n + \mathbf{\Phi}_0(\overline{\delta}T)\mathbf{\Psi}_1(\delta T) + \mathbf{\Psi}_0(\overline{\delta}T), & \text{for Case 1} \\ \mathbf{P}(\mathbf{x}_n, d_n) = \mathbf{\Phi}_0(\overline{d}_n T)\mathbf{\Phi}_1(d_n T)\mathbf{x}_n + \mathbf{\Phi}_0(\overline{d}_n T)\mathbf{\Psi}_1(d_n T) + \mathbf{\Psi}_0(\overline{d}_n T) & \text{for Case 2} \\ \mathbf{P}(\mathbf{x}_n, 1) = \mathbf{\Phi}_1(T)\mathbf{x}_n + \mathbf{\Psi}_1(T) & \text{for Case 3} \end{cases} \tag{14}$$

where $\overline{\delta} = 1 - \delta$ and $\overline{d}_n = 1 - d_n$. The accuracy of the obtained simplified model has been checked by comparing the bifurcation diagram obtained from this model and the one depicted in Fig. 5, which was obtained by using the model of the PV system supplied by a nonlinear PV generator. The bifurcation diagram obtained from the map corresponding to the simplified discrete-time model is depicted in Fig. 6. One can see that the agrement between this figure and Fig. 5 is very good. It has been checked that it is almost always the case for the rest of other DC bus voltage values.

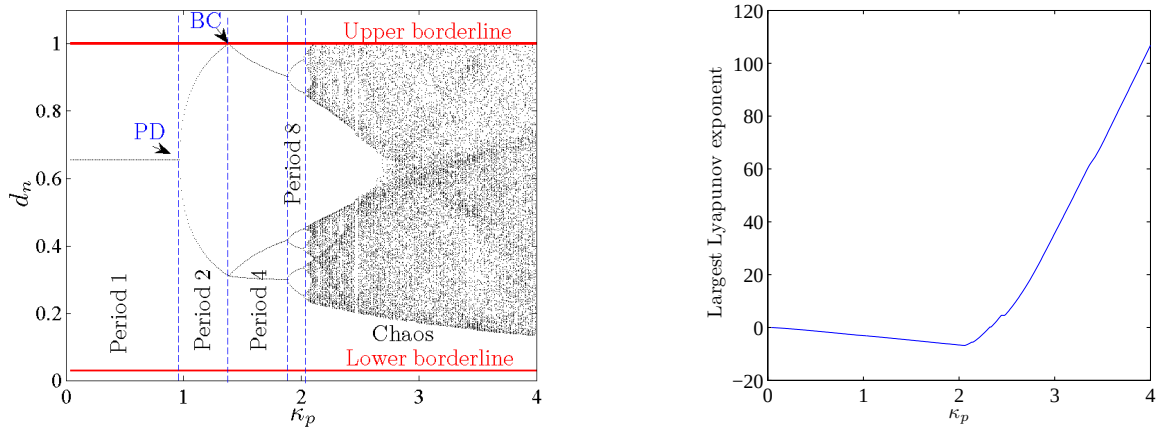

(a) (b)

Fig. 6. (a) Bifurcation diagram of the PV-fed boost converter showing the duty cycle d_n at time instants nT by taking the proportional gain κ_p as a bifurcation parameter. (b) Largest Lyapunov exponent.

It is worth noting here that the desired period-1 orbit is described only by the first equation in (14). However, when the stability of this orbit is lost, skipped cycles may take place and the model of the system changes according to the previous expression. Note that multiple pulsing during a switching cycle are

avoided during a switching cycle and hence there is only one and one value of d_n for each switching period. The expression of the Jacobian matrix of the previous model can be expressed as follows:

$$\mathbf{DP} = \begin{cases} \mathbf{DP}_\delta = e^{\mathbf{A}_0(1-\delta)T} e^{\mathbf{A}_1 \delta T} & \text{for case 1} \\ \mathbf{DP}_d = e^{\mathbf{A}_0(1-d_n)T} \mathbf{S} e^{\mathbf{A}_1 d_n T)} & \text{for case 2} \\ \mathbf{DP}_1 = e^{\mathbf{A}_1 T} & \text{for case 3} \end{cases} \tag{15}$$

where $\mathbf{S}$ is the saltation matrix defined as follows [Giaouris *et al.* , 2008, 2009; Giaouris *et al.*, 2013]

$$\mathbf{S} = \mathbf{I} + \frac{(\mathbf{f}_0(\mathbf{x}(d_n T)) - \mathbf{f}_1(\mathbf{x}(d_n T))\mathbf{K}}{\mathbf{K}\mathbf{f}_1(\mathbf{x}(d_n T)) - m_a} \tag{16}$$

where $\mathbf{f}_1(\mathbf{x}) = \mathbf{A}_1\mathbf{x}+\mathbf{B}$, $\mathbf{f}_0(\mathbf{x}) = \mathbf{A}_0\mathbf{x}+\mathbf{B}$ and $m_a = V_M f_s$ is the slope of the ramp modulator, $V_M = V_u - V_l$ being its amplitude, and $\mathbf{x}(d_n T) = \mathbf{\Phi_1}(d_n T)\mathbf{x}_n + \mathbf{\Psi_1}(d_n T)$ the state vector at time instant $d_n T$. The parameter d_n stands for the operating duty cycle. The presence of chaotic behavior can be demonstrated by calculating the Lyapunov exponents. Figure 6-(b) shows the the largest Lyapunov exponents as the bifurcation parameter is varied by using the algorithm detailed in [Wolf *et al.*, 1985]. Chaotic behavior is evidenced by the presence of a positive exponent.

6. Stability analysis of the period-1 orbit

The stability of periodic orbits of a closed loop PV system can be analyzed by checking the evolution of a small perturbation in the state variable within one period. This problem can be tackled by different ways. One of the most used techniques is to analyze the stability of the fixed points of the Poincaré map of the closed loop system by using its Jacobian matrix. The periodic orbit will be stable if this matrix evaluated at the associated fixed point has eigenvalues with modulus less than 1. Another technique is by using Floquet theory combined with Filippov method which leads to the same results [Giaouris *et al.* , 2008, 2009; Giaouris *et al.*, 2013]. The Jacobian matrix $\mathbf{DP}_d$ derived in (15) coincides with the monodromy matrix $\mathbf{M}_d$ of the period-1 orbit. In order to locate the critical value of the gain for which the useful period-1 regime loses its stability, the eigenvalues of the monodromy matrix are calculated by substituting $\mathbf{x_n}$ and d_n in (15) by their steady-state values in the period-1 regime. By varying the gain κ_p, the operating point of the system was calculated and the monodromy matrix was evaluated at this point. Its eigenvalues are obtained and are represented in the complex plane for the different values of κ_p hence obtaining the root locus of the system. The results are depicted in Fig. 7 which shows that one of the eigenvalues crosses the unit circle at $\kappa_p \approx 0.99$ from the point $(-1, 0)$ in the complex plane while the other remaining eigenvalues barely change when varying κ_p. Hence, the system undergoes a period-doubling bifurcation for $\kappa_p \approx 0.99$.

In order to locate the stability boundary of the desired period-1 regime and subharmonic oscillation one can use the expression of the characteristic equation $\det(\mathbf{DP}_d - \lambda\mathbf{I}) = 0$, impose the period doubling condition in the eigenvalue λ and solve the resulting equation together with the steady-state condition. Namely, at a point where a period-2 orbit is born, one of the eigenvalues of $\mathbf{DP}_d$ is equal to -1. Therefore at the boundary corresponding to this singular point, the following condition is fulfilled

$$\det(\mathbf{DP}_d + \mathbf{I}) = 0 \tag{17}$$

This equation will be used later to obtain the stability boundary of the system using the simplified discrete-time model and the results will be compared with those obtained from time-domain numerical simulations using the switched circuit-level model and experimental measurements from a laboratory prototype.

7. Experimental validation

An experimental set up for the system is developed to verify the numerical simulations from PSIM© and the theoretical derivation from the stability analysis using the monodromy matrix presented previously. A picture of the implemented converter and its controller are depicted in Fig. 8. The circuit parameter are the ones shown Table 1 and Table 2. A PV emulator AGILENT E4361A was used as PV source allowing to obtain repeatable experiments. The inductor was built with toroidal Magnetics Kool-mu© and

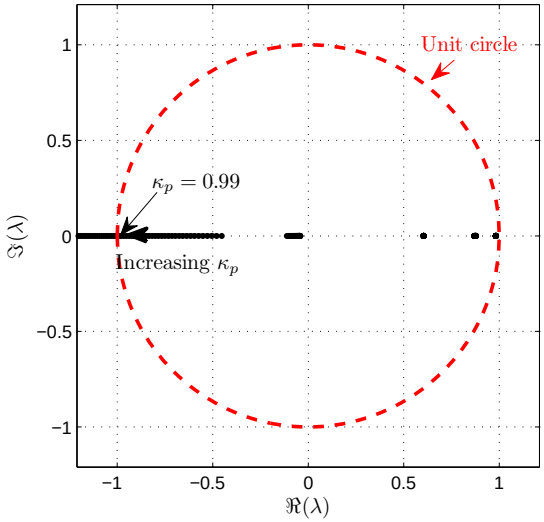

Fig. 7. Eigenvalues of the monodromy matrix of the boost-based LFR when the parameter κ_p is varied within the range (0.7,1.2)

its inductance value is 200 μH. The output capacitor is the parallel connection of five metallized polyester (MKT) capacitors, each of a capacitance of 10 μF, and seventy ceramic (X7R) capacitors with a capacitance of 2.2 μF each. The total nominal capacitance is 204 μF. The input capacitor is the parallel connection of one 10 μF metallized polyester (MKT) capacitor and fifteen 2.2 μF ceramic (X7R) capacitors. The total input capacitance is 43 μF. The switch used is an IRFP4110PBF Silicon MOSFET and the diode is a MBR30H100CTG Silicon Schottky diode. The rated voltage of all the capacitors, switch and diode is 100 V. The inductor current sensing was carried out by an LEM LA25-NP Hall effect current transducer. The emulator was set with an open circuit voltage $V_{oc} = 22.1$ V, an MPP voltage $v_{\text{mpp}} = 18$ V, a short circuit current $I_{\text{sc}} = 5$ A and an MPP current $i_{\text{mpp}} = 4.72$ A. In order to emulate an ideal constant voltage sink at the converter output, an electronic load (ELEKTRO-AUTOMATIK EL3400-25) was used. The duty ratio was varied by adjusting the load voltage. To obtain the LFR behavior, the input current and voltage are controlled to be proportional. For that purpose, a current reference was generated by multiplying, using an analog multiplier (AD633JNZ), the PV panel voltage by a signal from signal generator Tektronix AFG2021 which emulates the conductance g. Subtracting the inductor current from the reference, we obtain the error which is processed by a type-II controller. The output of this controller is compared with a 50 kHz sawtooth ramp signal provided from another signal generator Tektronix AFG2021. When the ramp signal is larger than the control signal, the comparator LM319N forces the SR flip-flop CD4027BE to reset, and the driving signal will be zero. At the end of each period of the ramp, another comparator LM3l9N forces a set for the SR flip-flop, placing the driving signal to 1. The output of the SR flip-flop is the switch driving signal by means of the driver MCP1407-E/P. The results, shown below, have been measured by using the oscilloscope Tektronix TDS 754C and the probes TEKTRONIX TCP202 for illustrating the current waveforms.

Fig. 9 shows the waveforms of the control signal, ramp signals, and the inductor current for different values of the controller gain. It can be clearly seen in this figure that by increasing the proportional gain κ_p, the converter presents a cascade of period doubling bifurcation leading to chaotic mode of operation. In fact, for $\kappa_p = 0.8$, the system operates in a stable periodic-1 regime. By increasing κ_p to 1.1, a period-2 orbit appears. Additionally, by taking $\kappa_p = 1.4$, a period-4 orbit is obtained. Further increase in the gain value, $\kappa_p = 2.5$, leads to the occurrence of the chaotic regime. From the results in the previous section, it has been shown that the system can result in undesired bifurcation behavior if the parameter values are varied. The boundary between the desired period-1 orbit and subharmonic oscillation resulting from period doubling in the parameter space is obtained using both nonlinear PV generator and current source models. It can be shown that for each value of the duty cycle D, the system is stable if the gain κ_p is smaller than a

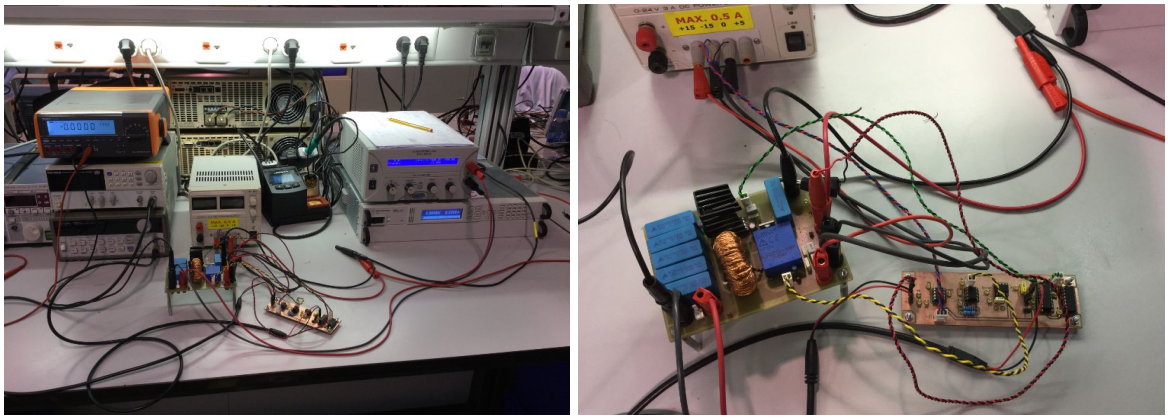

(a) (b)

Fig. 8. Implementation of the current-fed boost converter: (a) the overall system, (b) the power board.

critical value which as a function of D presents a maximum in the vicinity of $D = 0.3$. Some discrepancies between the results can be appreciated. First, by approximating the nonlinear PV generator model by a current source, the range of stability is slightly smaller than when the nonlinear model is used. However, the error committed by the approximation can be neglected for all the range of duty cycle values. The discrepancy between the simulation results and the experimental results can be attributed to uncertainties in the parameters and some parasitic parameters not included in the modeling.

One can observe that for relatively low values of the duty cycles (< 0.3), there is some discrepancies between the results obtained form the simplified model and the one using the nonlinear model of the PV panel. Namely, for the same value of the duty cycle, the critical value of the proportional gain for the system to loss its stability is larger for the last model. This is in agreement with [Al-Hindawi *et al.* , 2014] where it has been stated that the inherent nonlinearity present in the system due to the PV generator improves the stability of the system. For the rest of values of the duty cycle one can observe that the agreement between the results are remarkable. Note however that most of the discrepancies can be observed for low values of the duty cycle where the system is not supposed to work in PV applications.

Conclusion

In practice, switching mode DC-DC converters are designed to operate in a stable period-1 operation. However, switching aspect of such systems makes them complex and prone to exhibit instabilities in the form of bifurcations. In this paper, the dynamic behavior and stability analysis of a PV-fed boost converter for PV applications has been accurately addressed under a fixed frequency PWM control. In order to allow an analytical stability analysis, the PV generator has been approximated by a current source. This assumption has been validated by using the switched circuit-level model implemented in PSIM©. It has been shown by using bifurcation diagrams and PSIM© simulations that the first instability taking place in the system is a period-doubling bifurcation. The same qualitative behavior has been obtained if the PV generator model is substituted by a current source. This has justified the use of a simplified model to perform a stability analysis of the system periodic behavior. By calculating the eigenvalues of the monodromy matrix of the simplified model, the first period doubling has been detected and the stability region in the $D - \kappa_p$ parameter space has been obtained. This gives an overview of the stability range of the gain κ_p versus the duty cycle D and hence identifies the useful operating region of the PV system in the design parameter space. Experimental tests performed in the laboratory to the proposed system are in good agreement with the simulation results and show that the PV-fed boost-based LFR exhibits period doubling bifurcation when the proportional gain is varied being the nonlinearity of the PV generator irrelevant for the subharmonic oscillation prediction.

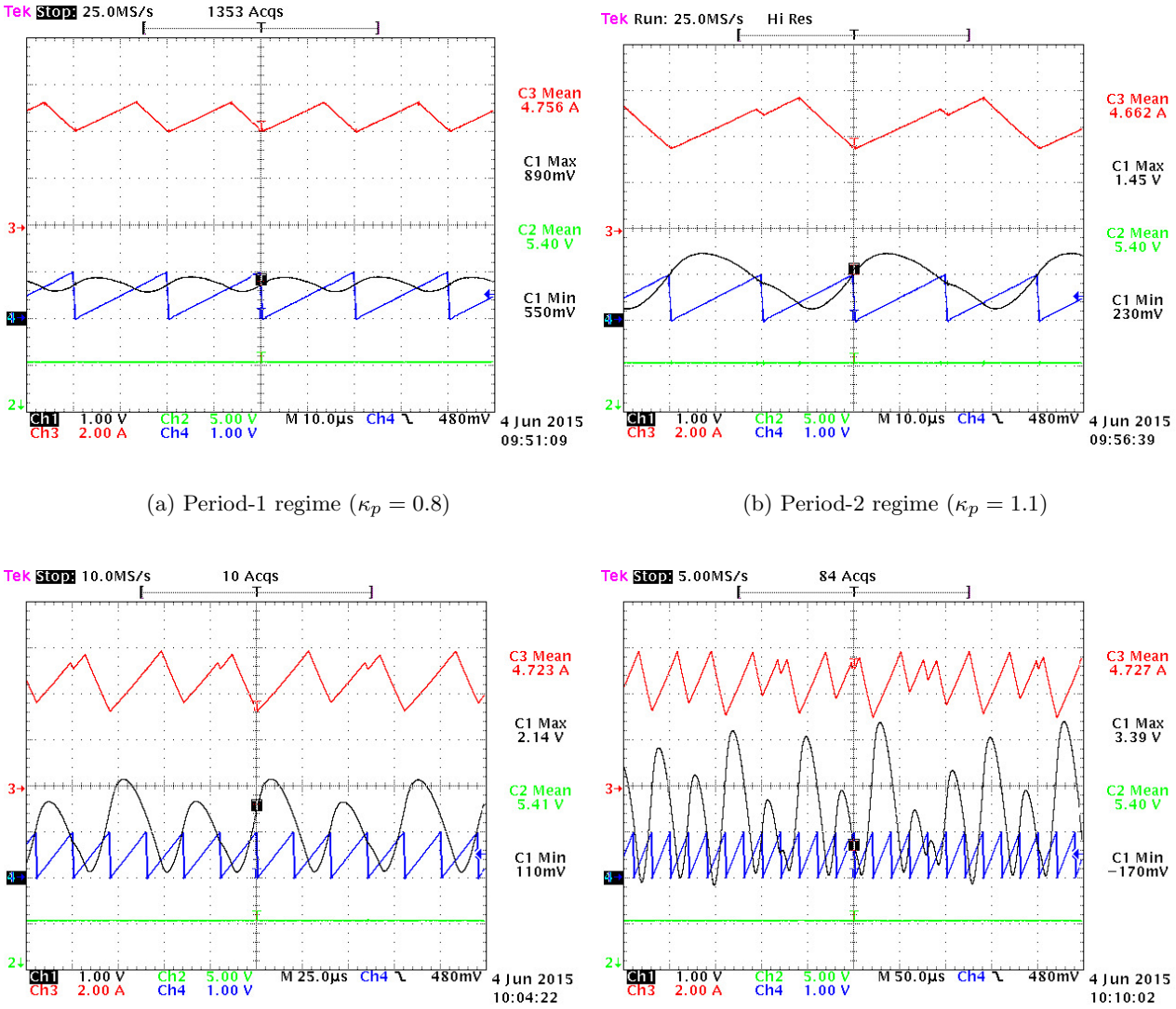

(a) Period-1 regime ($\kappa_p = 0.8$)

(b) Period-2 regime ($\kappa_p = 1.1$)

(c) Period-4 regime ($\kappa_p = 1.4$)

(d) Chaotic regime ($\kappa_p = 2.5$)

Fig. 9. Experimental responses of the boost-based LFR for different value of the proportional gain κ_p.

References

Xiao, W., Dunford, W. G., Palmer, P. R., & Capel, A. [2007] "Regulation of photovoltaic voltage," *Industrial Electronics, IEEE Transactions on* **54**, 1365–1374.

Available at ⟨http://www.epia.org/fileadmin/user_upload/Publications/EPIA_Global_Market_Outlook_for_Photovoltaics_2014-2018_-_Medium_Res.pdf⟩

Leyva, R.,Alonso, C., Queinnec, I., Cid-Pastor, A., Lagrange, D., & Martinez-Salamero, L. [2006] "Mppt of photovoltaic systems using extremumseeking control," *IEEE Trans. Aerosp. Electron. Syst.*, **42**, 249–258.

Yang, S., Goto, K., Imamura, Y., & Shoyama, M. [2012] "Dynamic characteristics model of bi-directional DC-DC converter using state-space averaging Method," *Telecommunications Energy Conference (INTELEC), IEEE 34th International,*, 1–5.

Chiu, H. J., Lo, Y. K., Lee, T. P., Chen, Q. S., Yu, W. L., Lee, J. X., ... & Mou, S. C. [2011] "A battery charger with maximum power point tracking function for low-power photovoltaic system applications," *International Journal of Circuit Theory and Applications*, **39**, 241–256.

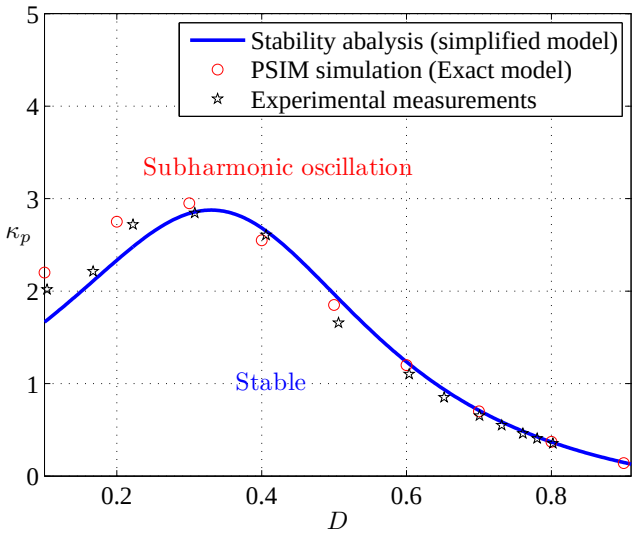

Fig. 10. The stability region of the system in the (D,κ_p) parameter space.

Garcer, G., Gonzlez-Medina, R., Figueres, E., & Sandia, J. [2012] "Dynamic modeling of DC-DC converters with peak current control in double-stage photovoltaic grid-connected inverters," *International Journal of Circuit Theory and Applications*, **40**, 793–813.

Deane, J. H. [1992] "Chaos in a current-mode controlled boost DC-DC converter," *IEEE Transactions on circuits and systems - I: Fundamental theory and applications*, **39**, 680–683.

Deane, J. H., & Hamill, D. C. [1990] "Analysis, simulation and experimental study of chaos in the buck converter," *IEEE Power Electronics Specialists Conference*, **2**, 491–498.

Deane, J. H., & Hamill, D. C. [1991] "Chaotic behaviour in current-mode controlled DC-DC convertor," *Electronics Letters*,**27**, 172–1173.

Deane, J. H., & Hamill, D. C. [1990] "Instability, subharmonics, and chaos in power electronic systems," *Power Electronics, IEEE Transactions on*, **5**, 260–268.

Dénes, I., & Nagy, I. [2003] "Two models for the dynamic behavior of a dual-channel buck and boost DC-DC converter," *Electromotion*, **10**, 556–561.

Fossas, E., & Olivar, G. [1996] "Study of Chaos in the Buck Converter," *IEEE Transactions on circuits and systems - I: Fundamental theory and applications,* **43**, 13–25.

Banerjee, S., & Verghese, G. [2001] " Nonlinear phenomena in power electronics: attractors, bifurcations chaos, and nonlinear control," *New York: IEEE Press.*

El Aroudi, A., Debbat, M., Giral, R., Olivar, G., Benadero, L., & Toribio, E. [2005] "Bifurcations in DC-DC Switching Converters Review of Methods and Applications," *International Journal of Bifurcation and Chaos,***15**, 1549–1578.

Banerjee, S., & Chakrabarty, K. [1998] "Nonlinear modeling and bifurcations in the boost converter," *Power Electronics, IEEE Transactions on*, **13**, 252–260.

El Aroudi, A., & Leyva, R. [2001] "Quasi-periodic route to chaos in a pwm voltage-controlled DC-DC boost converter," *IEEE Transactions on circuits and systems - I: Fundamental theory and applications,* **48**, 967–978.

Zhusubaliyev, Z. T., Soukhoterin, E. A., & Mosekilde, E. [2003] "Quasi-periodicity and border-collision bifurcations in a DC-DC converter with pulsewidth modulation," *IEEE Transactions on circuits and systems - I: Fundamental theory and applications,* **50**, 1047–1057.

Chan, W. C., & Tse, C. K. [1997] "Study of bifurcations in current-programmed dc/dc boost converters: from quasiperiodicity to period-doubling," *IEEE Transactions on circuits and systems - I: Fundamental theory and applications,* **44**, 1129–1142.

Cafagna, D., & Grassi, G. [2006] "Bifurcation analysis and chaotic behavior in boost converters: experi-

mental results," *Nonlinear Dynamics* , **44**, 1–4.

Pikulin, D. [2014]"Complete bifurcation analysis of DC-DC converters under current mode control," *Journal of Physics: Conference Series*, **482**, 012034.

Zamani, N., Ataei, M., & Niroomand, M. [2015] "Analysis and control of chaotic behavior in boost converter by ramp compensation based on Lyapunov exponents assignment: theoretical and experimental investigation," *Chaos, Solitons & Fractals*, **81**, 20–29.

Xiong, X., Tse, C. K., & Ruan, X. [2013] "Smooth and non-smooth bifurcations in multi-structure multi-operating-mode hybrid power systems," *International Journal of Bifurcation and Chaos,***23**, 1350094.

El Aroudi, A., Giaouris, D., Ho-Ching Iu, H., & Hiskens, I. A. [2015] "A Review on Stability Analysis Methods for Switching Mode Power Converters," *Emerging and Selected Topics in Circuits and Systems, IEEE Journal on*, **5**, 302–315.

Giaouris, D., Banerjee, S., Zahawi, B., & Pickert, V. [2008] "Stability Analysis of the Continuous-Conduction-Mode Buck Converter Via Filippov's Method," *IEEE Transactions on Circuits and Systems I: Regular Papers,* **55**, 1084–1096.

Giaouris, D., Maity, S., Banerjee, S., Pickert, V., & Zahawi, B. [2009] "Application of Filippov method for the analysis of subharmonic instability in DC-DC converters," *International Journal of Circuit Theory and Applications,* **37**, 899–919.

Giaouris, D., Banerjee, S., Stergiopoulos, F., Papadopoulou, S., Voutetakis, S., Zahawi, B., ... & Al-Turki, Y. [2013] "Foldings and grazings of tori in current controlled interleaved boost converters," *International Journal of Circuit Theory and Applications,* **42**, 1080–1091.

Tse, C. K., & Li, M. [2011] " Design-oriented Bifurcation analysis of power Electronics Systems," *International Journal of Bifurcation and Chaos,* **21**, 1523–1537.

Al-Hindawi, M. M., Abusorrah, A., Al-Turki, Y., Giaouris, D., Mandal, K., & Banerjee, S. [2014] "Nonlinear dynamics and bifurcation analysis of a boost converter for battery charging in photovoltaic applications," *International Journal of Bifurcation and Chaos,* **24**, 1450142.

Abusorrah, A., Al-Hindawi, M. M., Al-Turki, Y., Mandal, K., Giaouris, D., Banerjee, S., ... & Papadopoulou, S. [2013]"Stability of a boost converter fed from photovoltaic source," *Solar Energy*, **98**, 458–471.

Zhioua, M., El Aroudi, A. & Belghith, S. [2015] "Analysis of bifurcation behavior in a current-fed boost converter for PV systems," *12th International Multi-Conference on Systems, Signals & Devices,* 1–6.

Shmilovitz, D. [2005]"On the control of photovoltaic maximum power point tracker via output parameters," *Electric Power Applications, IEE Proceedings*, **152**, 239–248.

Cid-Pastor, A., Martinez-Salamero, L., Parody, N., & Aroudi, A. E. [2010] "Analysis and design of a loss-free resistor based on a boost converter in PWM operation," *Proceedings of 2010 IEEE International Symposium on Circuits and Systems (ISCAS),*2742–2745.

Haroun, R., Cid-Pastor, A., El Aroudi, A., & Martinez-Salamero, L. [2014] "Synthesis of canonical elements for power processing in DC distribution systems using cascaded converters and sliding-mode control," *IEEE Transactions on Power Electronics,* **29**, 1366–1381.

Haroun, R., El Aroudi, A., Cid-Pastor, A., Garica, G., Olalla, C., & Martinez-Salamero, L. [2015]"Impedance matching in photovoltaic systems using cascaded boost converters and sliding-mode control," *IEEE Transactions on Power Electronics,* **30**, 3185–3199.

Villalva, M. G., & Gazoli, J. R. [2009] "Comprehensive approach to modeling and simulation of photovoltaic arrays," *IEEE Transactions on Power Electronics,* **24**, 1198–1208.

BP Solar BP585 Datasheet, [Online], Available: http://www.comel.gr/pdf/bpsolar/BP585.pdf.

Banerjee, S., Ott, E., Yorke, J. A., & Yuan, G. H. [1997] "Anomalous bifurcations in DC-DC converters: borderline collisions in piecewise smooth maps," *IEEE Power Electronics Specialists Conference,* 1337–1344.

Banerjee, S., Ranjan, P., & Grebogi, C. [2000] "Bifurcations in two-dimensional piecewise smooth maps-theory and applications in switching circuits," *IEEE Transactions on Circuits and Systems-I* **47**, 633–643.

Robert, B., & Robert, C. [2002] "Border Collision Bifurcations in a One-Dimensional Piecewise Smooth Map for a PWM Current-Programmed H-Bridge Inverter," *International Journal of Control*,**75**, 1356–

1367.

Wolf, D. M., Varghese, M., & Sanders, S. R. [1994] "Bifurcation of Power Electronic Circuits," *Journal of Franklin Institute*, **331**, 957–999.

Leppäaho, J., Nousiainen, L., Puukko, J., Huusari, J., & Suntio, T. [2010] " Implementing Current-Fed Converters by Adding an Input Capacitor at the Input of Voltage-Fed Converter for Interfacing Solar Generator," *International Power Electronics and Motion Control Conference*, pp. 81–88.

Leppaaho, J., & Suntio, T. [2011] "Dynamic Characterization of Current-Fed Superbuck Converter," *IEEE Transactions on Power Electronics,* **26** , 200–209.

Wolf, A., Swift, J. B., Swinney, H. L., & Vastano, J. A. [1985] "Determining Lyapunov exponents from a time series," *Physica D: Nonlinear Phenomena*, **16**, 285–317.

El Aroudi, A., Debbat, M., & Martinez-Salamero, L. [2007] "Poincaré Maps Modelling and Local Orbital Stability Analysis of Discontinuous Piecewise Affine Periodically Driven Systems", *Nonlinear Dynamics,* **50**, 431–445.